Eur. Phys. J. B **30**, 487–494 (2002)
DOI: 10.1140/epjb/e2002-00405-5

THE EUROPEAN PHYSICAL JOURNAL B

Interplay of charge, spin, orbital and lattice correlations in colossal magnetoresistance manganites

A. Weiße[1,a] and H. Fehske[2]

[1] Physikalisches Institut, Universität Bayreuth, 95440 Bayreuth, Germany
[2] Institut für Physik, Ernst-Moritz-Arndt Universität Greifswald, 17487 Greifswald, Germany

Received 4 September 2002 / Received in final form 8 November 2002
Published online 31 December 2002 – © EDP Sciences, Società Italiana di Fisica, Springer-Verlag 2002

Abstract. We derive a realistic microscopic model for doped colossal magnetoresistance manganites, which includes the dynamics of charge, spin, orbital and lattice degrees of freedom on a quantum mechanical level. The model respects the $SU(2)$ spin symmetry and the full multiplet structure of the manganese ions within the cubic lattice. Concentrating on the hole doped domain ($0 \leq x \leq 0.5$) we study the influence of the electron-lattice interaction on spin and orbital correlations by means of exact diagonalisation techniques. We find that the lattice can cause a considerable suppression of the coupling between spin and orbital degrees of freedom and show how changes in the magnetic correlations are reflected in dynamic phonon correlations. In addition, our calculation gives detailed insights into orbital correlations and demonstrates the possibility of complex orbital states.

PACS. 71.10.-w Theories and models of many-electron systems – 71.38.-k Polarons and electron-phonon interactions – 75.30.Vn Colossal magnetoresistance

1 Introduction

The observation of the colossal magnetoresistance effect (CMR) [1–3] in doped manganese oxides with perovskite structure, $R_{1-x}A_xMnO_3$ (R = rare-earth, A = alkaline-earth metal), moved these materials into the focus of intense research activity [4–6]. It turned out soon that the complex electronic and magnetic properties of the manganites depend on a close interplay of almost all degrees of freedom known in solid state physics, namely itinerant charges, localised spins, orbitals, and lattice vibrations. On the one hand, the strong Coulomb interaction U and the Hund's rule coupling J_h introduce a spin background and affect the charge mobility *via* double-exchange [7–9]. On the other hand, the cubic environment of the Mn sites within the perovskite lattice results in a crystal field splitting of Mn-d-orbitals into e_g and t_{2g} and gives rise to an orbital degeneracy in the ground-state of Mn^{3+} ions. This orbital degeneracy, in turn, connects the electronic system to the lattice, making it sensible to Jahn-Teller distortion and polaronic effects [10].

There are numerous attempts to describe the electronic (*i.e.*, charge, spin, and orbital) interactions of the manganites on a microscopic level (see, *e.g.*, Refs. [11–13]). However, most of these models do not reflect the full multiplet structure of the Mn ions caused by the cubic site symmetry or violate the spin rotational invariance. To our knowledge, Feiner and Olés [14] were the first who derived a consistent spin-orbital model for the undoped compounds. In the following we extend their derivation to the case of finite doping and complete the resulting electronic model with dynamic electron-lattice interactions of Jahn-Teller and breathing type. Up to now models of similar complexity have only been discussed on the basis of rather extensive approximations, where mean-field approaches are probably the most popular. In particular, the lattice was always treated within the adiabatic approximation which is questionable in view of the comparable energy scales of spins and phonons. For a better understanding of this complex many body system we prefer to consider all interactions on an equal footing. Using exact diagonalisation techniques we study the ground-state properties of the derived model on a four site cluster.

For the hole doped region ($0 \leq x \leq 0.5$) our calculations show how the lattice can effectively control the spin and orbital correlations and the charge mobility. In the undoped compounds the electron-phonon interaction suppresses the coupling of spin and orbital degrees of freedom and is most effective in determining orbital order. At doping $x = 0.25$, where ferromagnetism is stabilised by the double-exchange mechanism, the coupling to the lattice can cause self-trapping of the charge carriers, which

[a] e-mail: Alexander.Weisse@uni-bayreuth.de

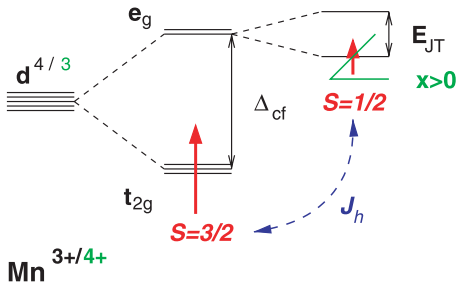

Fig. 1. Local electronic structure of Mn-d-electrons in a cubic environment. Here $\Delta_{\rm cf}$, J_h, and $E_{\rm JT}$ denote the crystal field splitting, the Hund's rule coupling, and the Jahn-Teller splitting, respectively.

immediately switches the spin order. In turn, this change is reflected in dynamic lattice correlations, namely the bond length fluctuation. For the half-doped manganites we find that the electron-phonon coupling enhances the susceptibility for charge ordering which is present already due to the strong Coulomb interaction. In addition, moderate variations in the strength of the electron-lattice coupling trigger pronounced changes in spin and orbital correlations. This relates to the complicated patterns of spin, charge and orbital ordering observed experimentally for different manganites at $x = 0.5$.

2 Microscopic model

2.1 Electronic interactions

The electronic and magnetic properties of the mixed-valence manganites are governed by the manganese d-electrons, which are divided into t_{2g} and e_g according to the cubic symmetry within the crystal field. Due to the large Coulomb and Hund's rule interactions each of the three t_{2g} and the two e_g levels carries at most one electron and the spins of several d-electrons are aligned in parallel at every site (see Fig. 1). Starting from the undoped compounds with only Mn^{3+} ions doping will remove e_g-electrons. Hence, the local electronic Hilbert space can be restricted to the large Hund's rule ionic ground-states of manganese ions in a cubic crystal field (see Ref. [15]). For Mn^{3+} (d^4) this corresponds to the spin-2 orbital doublet ${}^5E$ $[t_2^3({}^4A_2)e]$,

$$|\theta,2,m\rangle = +\sqrt{\tfrac{(2-m)!}{4!(2+m)!}}\,(S^+)^{(2+m)}\,c^\dagger_{\varepsilon\downarrow}c^\dagger_{\xi\downarrow}c^\dagger_{\eta\downarrow}c^\dagger_{\zeta\downarrow}|0\rangle$$
$$|\varepsilon,2,m\rangle = -\sqrt{\tfrac{(2-m)!}{4!(2+m)!}}\,(S^+)^{(2+m)}\,c^\dagger_{\theta\downarrow}c^\dagger_{\xi\downarrow}c^\dagger_{\eta\downarrow}c^\dagger_{\zeta\downarrow}|0\rangle\,, \quad (1)$$

and for Mn^{4+} (d^3) to the spin-$\frac{3}{2}$ orbital singlet ${}^4A_2$ $[t_2^3]$,

$$|a_2,\tfrac{3}{2},m\rangle = \sqrt{\tfrac{(\frac{3}{2}-m)!}{3!(\frac{3}{2}+m)!}}\,(S^+)^{(\frac{3}{2}+m)}\,c^\dagger_{\xi\downarrow}c^\dagger_{\eta\downarrow}c^\dagger_{\zeta\downarrow}|0\rangle\,. \quad (2)$$

Here the operators $c^\dagger_{\alpha\sigma}$ create spin σ electrons in the e_g ($\alpha = \theta,\varepsilon$) or t_{2g} ($\alpha = \xi,\eta,\zeta$) orbitals and $S^+ = \sum_\alpha c^\dagger_{\alpha\uparrow}c_{\alpha\downarrow}$ raises the on-site spin. The overlap of neighbouring manganese d and oxygen p orbitals allows for a tunneling of the manganese electrons between adjacent sites. Due to the specific symmetry of the involved orbitals this hopping acquires an anisotropy [16,17],

$$H_{\rm t} = -\sum_{i,\delta,\sigma} R_\delta \Big[t\, c^\dagger_{i,\theta\sigma}c_{i+\delta,\theta\sigma} + t_\pi(c^\dagger_{i,\xi\sigma}c_{i+\delta,\xi\sigma} + c^\dagger_{i,\eta\sigma}c_{i+\delta,\eta\sigma})\Big] + \text{h.c.}\,, \quad (3)$$

which can be expressed in terms of the spatial rotations

$$R_x = (C_3^d)^1\,,\ R_y = (C_3^d)^2 = (C_3^d)^{-1}\,,\ R_z = (C_3^d)^3 = 1$$
$$C_3^d : c_{\theta/\varepsilon} \to -\tfrac{1}{2}c_{\theta/\varepsilon} \pm \tfrac{\sqrt{3}}{2}c_{\varepsilon/\theta}\,;\ c_{\xi/\eta/\zeta} \to c_{\eta/\zeta/\xi}\,. \quad (4)$$

The transfer amplitudes t and t_π of e_g and t_{2g} electrons are small compared to the local energies U and J_h. Therefore the mobility of the e_g electrons depends on the correlations of the spin background formed by the t_{2g} electrons. Their kinetic energy is maximal, if neighbouring spins are aligned ferromagnetically, which is the essence of the well known double-exchange interaction [7,8]. Second order processes in t and t_π are responsible for numerous superexchange interactions between the localised spins, which inherit the orbital anisotropy of the hopping.

The electronic part of our model is derived by second order degenerate perturbation theory [14], *i.e.*, we calculated the matrix elements of $H_{\rm t}$ between the basis states (1) or (2) and all admissible excited states [15]. In Figure 2 the spin part of the fifteen different virtual excitations contributing to the superexchange is summarised graphically. We neglect terms which involve three different lattice sites. A compact expression for the resulting electronic Hamiltonian,

$$H_{\rm el} = \sum_{i,\delta} R_\delta (H^z_{i,i+\delta} + \text{h.c.})\,, \quad (5)$$

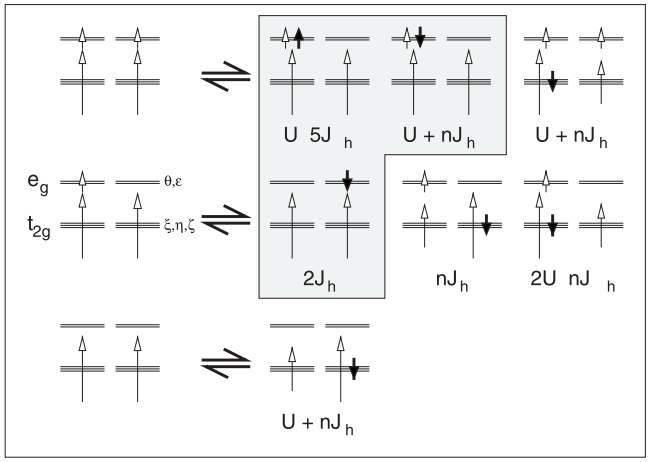

Fig. 2. Second order virtual excitations contributing to the model Hamiltonian $H_{\rm el}$, equation (5). The shaded region corresponds to t^2 terms, the other terms are proportional to t_π^2. n denotes different nonnegative prefactors of J_h (see Eq. (8)).

$$H^z_{i,j} = -\frac{t}{5}\left(a_{i,\uparrow}a^\dagger_{j,\uparrow} + a_{i,\downarrow}a^\dagger_{j,\downarrow}\right)\left(d^\dagger_{i,\theta}n_{i,\varepsilon}d_{j,\theta}n_{j,\varepsilon}\right) + t^2\,\frac{\mathbf{S}_i\mathbf{S}_j - 3}{32J_h}\,P^\varepsilon_i P^{a_2}_j - t^2\,\frac{\mathbf{S}_i\mathbf{S}_j + 6}{10(U-5J_h)}\,P^\varepsilon_i P^\theta_j$$
$$+ t^2\,\frac{\mathbf{S}_i\mathbf{S}_j - 4}{8}\left[\frac{(4U+J_h)\,P^\varepsilon_i P^\theta_j}{5U(U+\frac{2}{3}J_h)} + \frac{(U+2J_h)\,P^\varepsilon_i P^\varepsilon_j}{(U+\frac{10}{3}J_h)(U+\frac{2}{3}J_h)}\right] + t^2_\pi\,\frac{\frac{4}{9}\mathbf{S}_i\mathbf{S}_j - 1}{U+\frac{4}{3}J_h}\,P^{a_2}_i P^{a_2}_j$$
$$+ t^2_\pi\,\frac{\mathbf{S}_i\mathbf{S}_j - 3}{3}\left[\frac{(U-2J_h)(R_x(P^\varepsilon_i P^{a_2}_j) + R_y(P^\varepsilon_i P^{a_2}_j))}{\frac{19}{3}J_h(2U-\frac{7}{3}J_h)} + \frac{(U+\frac{5}{3}J_h)(R_x(P^\theta_i P^{a_2}_j) + R_y(P^\theta_i P^{a_2}_j))}{\frac{13}{3}J_h(2U-J_h)}\right]$$
$$+ t^2_\pi\,\frac{\mathbf{S}_i\mathbf{S}_j - 4}{8}\left[\frac{R_x(P^\varepsilon_i P^\varepsilon_j) + R_y(P^\varepsilon_i P^\varepsilon_j)}{U+8J_h/3} + \frac{R_x(P^\theta_i P^\theta_j) + R_y(P^\theta_i P^\theta_j)}{U+2J_h} + \frac{(2U+\frac{14}{3}J_h)(R_x(P^\varepsilon_i P^\theta_j) + R_y(P^\varepsilon_i P^\theta_j))}{(U+4J_h)(U+\frac{2}{3}J_h)}\right] \quad (8)$$

is obtained by rewriting the orbital and charge degrees of freedom of the basis states (1) and (2) in terms of new Fermi operators $d^\dagger_\alpha$ and projectors P^α,

$$|\theta\rangle = d^\dagger_\theta|0\rangle, \qquad |\varepsilon\rangle = d^\dagger_\varepsilon|0\rangle, \qquad |a_2\rangle = d^\dagger_\theta d^\dagger_\varepsilon|0\rangle,$$
$$P^\theta = n_\theta(1-n_\varepsilon), \quad P^\varepsilon = n_\varepsilon(1-n_\theta), \quad P^{a_2} = n_\varepsilon n_\theta. \quad (6)$$

Note that these projectors are related to the common pseudo-spin operators

$$\tau^z = \tfrac{1}{2}\sigma^z\,, \quad \tau^{x/y} = R_{x/y}(\tau^z) = \tfrac{1}{4}(-\sigma^z \mp \sqrt{3}\sigma^x)\,, \quad (7)$$

by the equation $R_\delta(P^{\theta/\varepsilon}) = \frac{1}{2} \pm \tau^\delta$. Since the amplitude of the on-site spin is different for the basis states (1) and (2), it is convenient to represent the spin degree of freedom by Schwinger bosons $a_\uparrow$ and $a_\downarrow$ which allow for a uniform description. Then, the spin operator is defined by $2\,\mathbf{S} = a^\dagger_\mu \boldsymbol{\sigma}_{\mu\nu} a_\nu$, but the amplitude is subject to the constraint $2\,|\mathbf{S}| = a^\dagger_\uparrow a_\uparrow + a^\dagger_\downarrow a_\downarrow = 4 - n_\theta n_\varepsilon$. Using this notation in z-direction the interaction between nearest-neighbour sites is given by,

see equation (8) above.

The first order in t corresponds to the well known double exchange interaction [7–9], which the authors discussed in detail recently [18]. The second order in t and t_π appears to be more involved, since the number of admissible virtual excitations is rather large (see Fig. 2). However, in all cases it is basically the product of a Heisenberg-type spin interaction and two orbital projectors. The energies of the virtual excitations depend, in general, on all three Racah parameters [15] A, B, and C. Applying the convention of reference [14] we define U and J_h in terms of $d^4d^4 \rightleftharpoons d^5(^4A_1)d^3$ and $d^4d^4 \rightleftharpoons d^5(^6A_1)d^3$ excitations. Together with the approximation [19] $C \approx 4B$ this yields $U = A + 22B$ and $J_h = 6B$. Typical estimates for these energies are $U \approx 6\ldots9$ eV and $J_h \approx 0.6\ldots0.8$ eV [20–23].

2.2 Electron-phonon interaction

Concerning the electron-lattice interaction we concentrate on the local environment of the manganese ions, namely the surrounding oxygen octahedra (see Fig. 3). At every site two optical phonon modes of E_g symmetry, q_θ and q_ε, couple to the orbital degree of freedom of the e_g electrons. In addition, a breathing-mode q_{a_1} is sensitive to the electronic density. To lowest order in the elongations $q_\alpha = b^\dagger_\alpha + b_\alpha$ ($\alpha \in \{\theta, \varepsilon, a_1\}$) this is modelled by the $E \otimes e$ Jahn-Teller Hamiltonian [24]

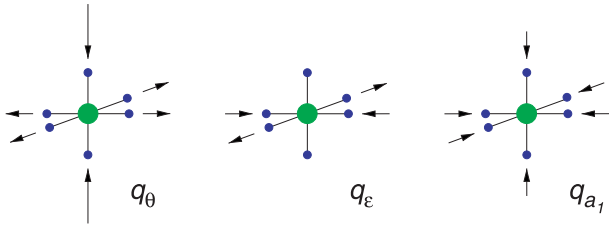

Fig. 3. Distortions of the oxygen octahedra for the Jahn-Teller (q_θ, q_ε) and the breathing-type (q_{a_1}) phonon modes.

$$H_{\mathrm{JT}} = g\sum_i \Big[(n_{i,\varepsilon} - n_{i,\theta})(b^\dagger_{i,\theta} + b_{i,\theta}) + (d^\dagger_{i,\theta}d_{i,\varepsilon} + d^\dagger_{i,\varepsilon}d_{i,\theta})(b^\dagger_{i,\varepsilon} + b_{i,\varepsilon})\Big] \quad (9)$$

and a Holstein-type [25] interaction

$$H_{\mathrm{br}} = \tilde{g}\sum_i (n_{i,\theta} + n_{i,\varepsilon} - 2n_{i,\theta}n_{i,\varepsilon})(b^\dagger_{i,a_1} + b_{i,a_1})\,. \quad (10)$$

The bosonic operators $b_{i,\alpha}$ describe the usual harmonic lattice dynamics,

$$H_{\mathrm{ph}} = \omega\sum_i \left[b^\dagger_{i,\theta}b_{i,\theta} + b^\dagger_{i,\varepsilon}b_{i,\varepsilon}\right] + \tilde{\omega}\sum_i b^\dagger_{i,a_1}b_{i,a_1}, \quad (11)$$

where we assume these phonons to be dispersion-less. At first glance the local structure of the electron-phonon interaction described by equations (9) to (11) does not seem to cover orbital-orbital interactions which are related to the displacement of intermediate oxygen ions. Inspection of the collective modes of the system shows, however, that the corresponding vibrations of the oxygen ions are of course present in our model. Consequently – as will become evident from the numeric data – this type of electron-phonon interaction causes an effective orbital-orbital interaction between neighbouring sites.

In experiments [26,27] the vibrational modes involving distortions of the oxygen octahedra are found to have frequencies of the order of 50 to 80 meV. For our calculations

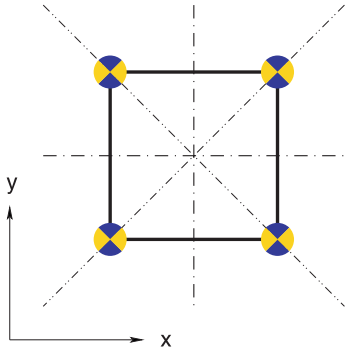

Fig. 4. Spatial symmetries of the considered cluster.

we assume $g = \tilde{g}$ and $\omega = \tilde{\omega}$ in addition to the neglected phonon dispersion. Apart from reducing the number of model parameters these approximations are reasonable, since we study a small finite system and are mainly interested in qualitative features of the electron-lattice interaction.

3 Numerical results

The Hilbert space of the complete microscopic model,

$$H = H_{\mathrm{el}} + H_{\mathrm{JT}} + H_{\mathrm{br}} + H_{\mathrm{ph}}, \tag{12}$$

is large and grows rapidly with the system size. However, using a density matrix based optimisation procedure [28] for the phonon subsystem we are able to retain the full quantum dynamics of the lattice and the electronic subsystem in our numerical calculation [29] of the ground-state properties. In addition we take into account some of the discrete symmetries of the model, namely the conservation of the S^z component of the spin, the particle number conservation, and the mirror symmetries orthogonal to the x and y axes (dot-dashed in Fig. 4). Nevertheless, the typical dimension of the eigenvalue problem is of the order of 10^6 and its repeated solution during the phonon optimisation requires the use of large scale computers.

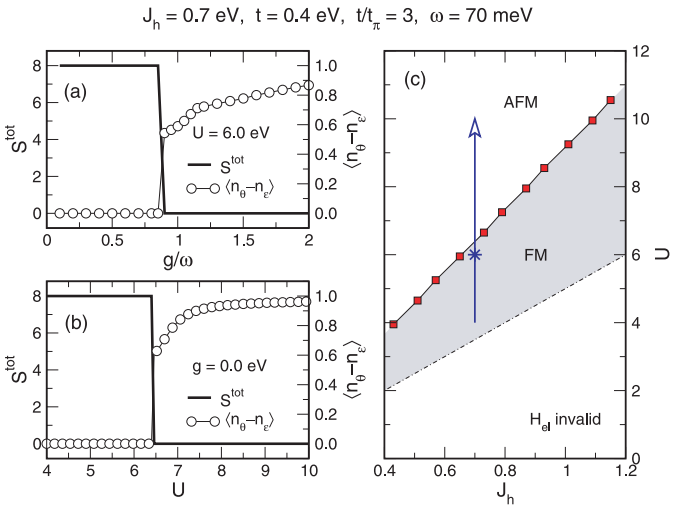

Fig. 5. Left: Total spin S^{tot} and orbital order ($\propto \langle n_\theta - n_\varepsilon \rangle$) of the ground-state of the cluster in dependence on (a) the electron-phonon coupling g, and (b) the Coulomb interaction U. Right: Phase diagram of the electronic model without electron-phonon interaction ($g = 0$).

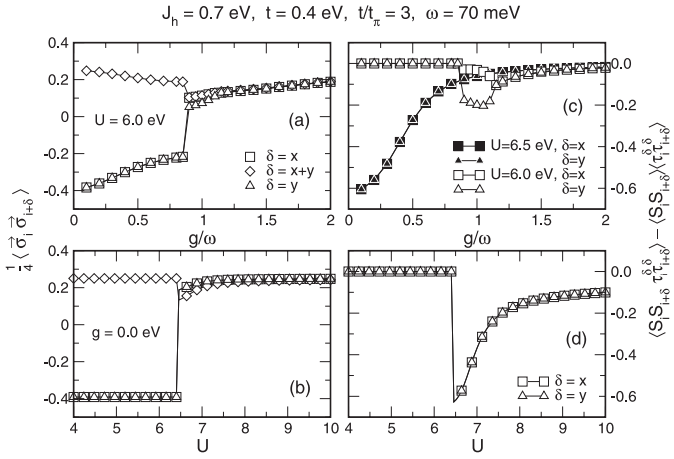

Fig. 6. Orbital-exchange (panels (a) and (b)) and spin-orbital (panels (c) and (d)) correlations between nearest and next-nearest neighbouring sites at variable electron-phonon coupling g and Coulomb interaction U.

3.1 Undoped manganites

The undoped manganese oxides ($\mathrm{LaMnO_3}$, $\mathrm{PrMnO_3}$) usually exhibit A-type anti-ferromagnetic order and strong Jahn-Teller distortion of the ideal perovskite structure [30,31]. The origin of the observed magnetic order has been subject to discussions. While different band structure calculations [32–35] emphasise the importance of lattice distortions for the stability of anti-ferromagnetism, Feiner and Oleś [14] favoured a purely electronic mechanism.

Our calculation points out that both parameters, U/J_h and g, can drive a transition from ferromagnetic (FM) to anti-ferromagnetic (AFM) order. Figure 5c shows the phase diagram of the electronic model without electron-phonon interaction, *i.e.*, $g = 0$. We assume $t = 0.4$ eV and $t/t_\pi = 3$ for the hopping integrals [14] and characterise the magnetic phases according to the total spin S^{tot} of the ground-state of the four site cluster. Parameters in the range $U \leq 5J_h$ implicate that for two neighbouring sites a d^5d^3 configuration becomes the ground-state in favour of the $d^4(^5E)d^4(^5E)$ configuration. This is incompatible with the situation in the manganites and consequently the electronic Hamiltonian H_{el} is not applicable for these values of U and J_h. Starting from the FM phase with $5J_h \leq U \lesssim 9.2J_h$ both, increasing U or g, change the magnetic order of the ground-state to AFM (Fig. 5a and b). The magnetic transition is accompanied by a change in the corresponding orbital order, which we identify by the local expectation value $\langle n_\theta - n_\varepsilon \rangle$ and the orbital exchange correlation $\langle \boldsymbol{\sigma}_i \boldsymbol{\sigma}_{i+\delta} \rangle$ between neighbouring sites. Here the Pauli matrices $(\sigma_i^\delta)_{\mu\nu}$ operate on the orbital degree of freedom, $\mu, \nu \in \{\theta, \varepsilon\}$, at the site i. The panels (a) and (b) of

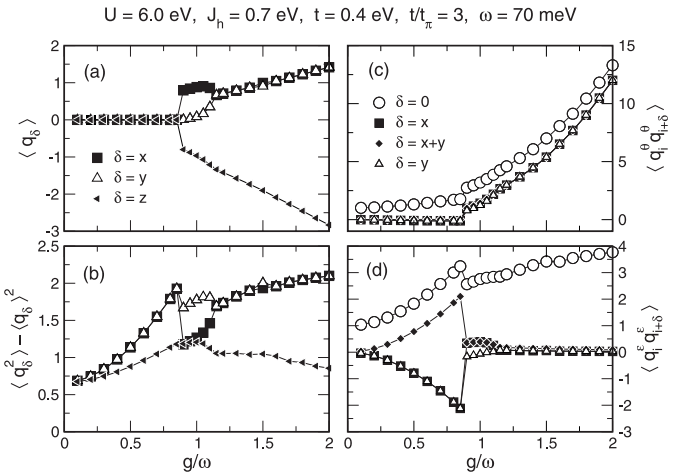

Fig. 7. Behaviour of the lattice with increasing electron-phonon coupling g: (a) expectation value, and (b) fluctuation of the bond lengths q_δ; (c) and (d) correlations of the Jahn-Teller modes q_θ and q_ε between different sites.

the Figures 5 and 6 illustrate the transition from staggered to uniform orbital order.

In view of the distinct driving interactions (U or g) both transitions appear to be very similar. However, we observe a significant difference, if we study the (de)coupling of spin and orbital degrees of freedom. The latter has been a rather controversial issue in the case of the Kugel-Khomskii model [36],

$$H = J \sum_{\langle ij \rangle_\delta} \left[4(\mathbf{S}_i \mathbf{S}_j) \left(\tau_i^\delta + \frac{1}{2} \right) \left(\tau_j^\delta + \frac{1}{2} \right) + \left(\tau_i^\delta - \frac{1}{2} \right) \left(\tau_j^\delta - \frac{1}{2} \right) - 1 \right], \quad (13)$$

which contains the same kind of spin-orbital interactions $\mathbf{S}_i \mathbf{S}_j \, \tau_i^\delta \tau_j^\delta$ as our Hamiltonian. Using equation of motion approaches for the approximate solution of the model (13) Khaliullin and Oudovenko [37] decoupled spin and orbital degrees of freedom, while Feiner *et al.* [38] emphasised the role of mixed spin-and-orbital excitations. A correlation function, which makes it possible to distinguish between these two decoupling schemes, is the spin-orbital fluctuation $\langle \mathbf{S}_i \mathbf{S}_{i+\delta} \, \tau_i^\delta \tau_{i+\delta}^\delta \rangle - \langle \mathbf{S}_i \mathbf{S}_{i+\delta} \rangle \langle \tau_i^\delta \tau_{i+\delta}^\delta \rangle$. The data we calculated for the complete manganite model (12) is given in Figures 6c and d. It indicates that this correlation is smaller by a factor of 3 to 5 if phonons are responsible for the FM to AFM transition (open symbols). On the other hand, starting within the AFM phase increasing electron-phonon interaction clearly suppresses the spin-orbital-fluctuation (Fig. 6c, bold symbols). This behaviour is, of course, crucial for effective theories that are based on such decoupling schemes.

To characterise the behaviour of the lattice we calculate the correlations $\langle q_{i,\alpha} q_{j,\alpha} \rangle$ ($\alpha \in \{\theta, \varepsilon\}$) between the elongations of the Jahn-Teller modes q_θ and q_ε at neighbouring sites i, j. The bond lengths

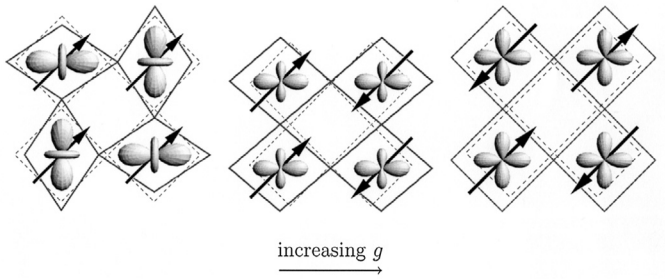

Fig. 8. Evolution of lattice, spin and orbital correlations with increasing electron-phonon coupling g at doping $x = 0$.

$$\begin{pmatrix} q_x \\ q_y \\ q_z \end{pmatrix} = \begin{pmatrix} \frac{1}{\sqrt{6}} & -\frac{1}{\sqrt{2}} & -\frac{1}{\sqrt{3}} \\ \frac{1}{\sqrt{6}} & \frac{1}{\sqrt{2}} & -\frac{1}{\sqrt{3}} \\ -\frac{2}{\sqrt{6}} & 0 & -\frac{1}{\sqrt{3}} \end{pmatrix} \cdot \begin{pmatrix} q_\theta \\ q_\varepsilon \\ q_{a_1} \end{pmatrix} \quad (14)$$

define additional significant quantities. In particular we considered the expectation values $\langle q_{i,\delta} \rangle$ and $\langle q_{i,\delta}^2 \rangle - \langle q_{i,\delta} \rangle^2$ with $\delta \in \{x, y, z\}$. Figure 7 shows that within the FM domain the lattice is undistorted but the q_ε vibrations are correlated along the (π, π) direction in reciprocal space. At intermediate values of $g/\omega \approx 1$ a finite x-y-distortion develops, which is also reflected in spin and orbital correlations (*e.g.*, the spin-orbital fluctuation in Figure 6c). Such type of asymmetry seems surprising in view of the invariance of the cluster with respect to diagonal reflections (dot-dot-dashed in Fig. 4). However, since this symmetry is not taken into account in the calculation the system is trapped in one particular linear combination of two degenerate ground-states and different expectation values in x and y direction can evolve. At larger electron-phonon coupling g only a finite q_θ distortion remains and the q_ε modes are uncorrelated.

In Figure 8 the change of orbital, spin and phonon correlations with increasing g is shown schematically. This, however, is a rather suggestive picture, which can not cover all the details of the various correlations. To select the appropriate graphical representation for the orbital arrangement we study the $E \otimes E$-eigenstates of reduced orbital density matrices. On a bond $\langle ij \rangle$ these states are either anti-symmetric,

$$|a\rangle_{ij} \propto (|\theta\rangle_i \otimes |\varepsilon\rangle_j - |\varepsilon\rangle_i \otimes |\theta\rangle_j) \,, \quad (15)$$

or symmetric,

$$|s(\varphi, \psi)\rangle_{ij} \propto (|\varphi\rangle_i \otimes |\psi\rangle_j + |\psi\rangle_i \otimes |\varphi\rangle_j) \,, \quad (16)$$

with respect to the permutation of two sites. The angles $\varphi, \psi \in \mathbb{C}$ parameterise two generalised orbital states of the form $|\varphi\rangle = \cos(\varphi)|\theta\rangle + \sin(\varphi)|\varepsilon\rangle$. At small g the staggered orbital order implies that the anti-symmetric orbital state is the most probable for each bond, *i.e.*, it belongs to the largest eigenvalue of the density matrix. Since an anti-symmetric combination of two arbitrary generalised states

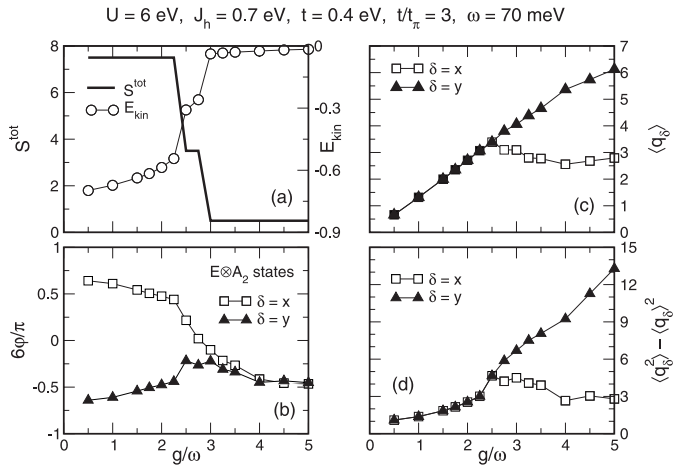

Fig. 9. Doping $x = 0.25$: (a) Total spin and kinetic energy *vs.* g; (b) generalised orbital states $|\varphi\rangle$ surrounding empty sites; (c) and (d) expectation value $\langle q_\delta \rangle$ and fluctuation $\langle q_\delta^2 \rangle - \langle q_\delta \rangle^2$ of the bond length in x and y direction.

$|\varphi\rangle$ and $|\psi\rangle$ is always proportional to $|a\rangle_{ij}$ the graphical representation remains undefined. Therefore we took into account also the second eigenstate of the density matrix, which is slightly less probable but necessarily symmetric. The associated angles φ and ψ define the orbital pattern shown in the left hand panel of Figure 8. For larger g the uniform orbital order allows for a calculation of the depicted orbital pattern directly from the most probable eigenstate of the density matrix. The spin arrangements are chosen such as to reflect the expectation values of the Heisenberg interaction, $\langle \mathbf{S}_i \mathbf{S}_j \rangle$, for nearest neighbour bonds $\langle ij \rangle$. Of course, the calculated ordering patterns can not be directly compared to experimental observations for the three dimensional compounds. Nevertheless, the orbital arrangement within the FM spin background closely resembles the data measured within the FM planes of the A-type AFM structure [39].

3.2 Doping x = 0.25

In view of the CMR effect the domain of low to intermediate doping ($0.15 \leq x \leq 0.5$) is certainly the most interesting one. Here ferromagnetism is stabilised by the double exchange interaction, which depends on the mobility of the charge carriers. However, if too strong electron-phonon coupling causes localisation of the holes, the spin order breaks down. For $x = 0.25$ our calculation of the ground-state properties clearly illustrates this coincidence. Figure 9a shows the total spin $S^{\rm tot}$ of the cluster together with the expectation value of the kinetic energy in the ground state,

$$E_{\rm kin} = \left\langle -\frac{t}{5} \sum_{i,\delta,\sigma} R_\delta \left[a_{i,\sigma} a^\dagger_{j,\sigma}\, d^\dagger_{i,\theta} n_{i,\varepsilon} d_{j,\theta} n_{j,\varepsilon} \right] + \text{h.c.} \right\rangle . \tag{17}$$

Obviously, the change from FM to AFM spin correlations with increasing electron-phonon interaction g is directly related to the charge mobility. In addition the transition is accompanied by the appearance of a lattice distortion in the x-y-plane (see Fig. 9c), which is interesting also in view of the lattice dynamics. Whereas one of the elongations, $\langle q_y \rangle$, grows linearly in g, the associated fluctuation $\langle q_y^2 \rangle - \langle q_y \rangle^2$ shows a kink near the FM to AFM transition point. This behaviour closely reminds the data collected by Booth *et al.* [40] using X-ray-absorption fine-structure measurements (XAFS). For $La_{1-x}Ca_xMnO_3$ these authors observed a similar rise in the Mn-O bond length variance σ^2 near the critical temperature of the transition from the ferromagnetic metallic to the paramagnetic insulating phase.

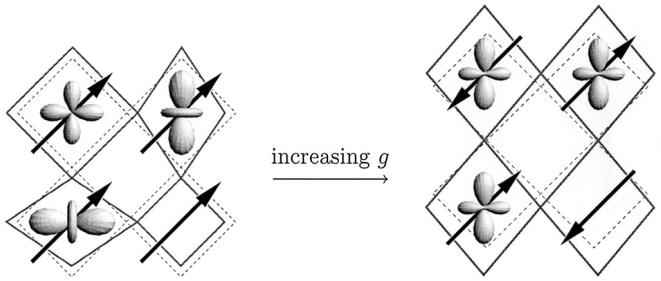

Fig. 10. Evolution of lattice, spin and orbital correlations with increasing electron-phonon coupling g at doping $x = 0.25$.

Orbital correlations are again extracted from the eigenstates of the reduced density matrices for a single bond. We concentrate on the environment of a hole, which is characterised by the $E \otimes A_2$ eigenstates, *i.e.*, by states describing a Mn^{3+} site neighbouring a Mn^{4+} site. Each of these states can be understood as the product $|\varphi\rangle_i \otimes |a_2\rangle_j$ of a generalised orbital state $|\varphi\rangle$ and the basis state $|a_2\rangle$ (see Eq. (2)). In Figure 9b the corresponding angle φ of the most probable eigenstate of the density matrix is given for bonds in x and y direction. The data for weak and strong electron-phonon coupling g is translated into the orbital arrangement presented in Figure 10. Increasing g reduces nearest-neighbour correlations and forces the orbital order to depend locally on the dominant electron-phonon interaction. The orbital polaron [41] pattern disappears, if the charge carrier is trapped completely.

3.3 Doping x = 0.5

At doping $x = 0.5$ the picture is more involved. Again we consider model parameters, which yield ferromagnetic spin correlations for vanishing electron-phonon coupling, $g = 0$. The strong Coulomb interaction U then leads to the formation of a charge density wave with ordering vector (π, π) in reciprocal space. Increasing electron-phonon coupling g amplifies this trend, and at large g the trapping of the carriers gives rise to charge order. In Figure 11c this is illustrated with the density-density correlation between different lattice sites i and j. From the model Hamiltonian (8) it is obvious that if charges tend to maximise their mutual distance the particular anti-ferromagnetic component of the Heisenberg spin interaction, which is

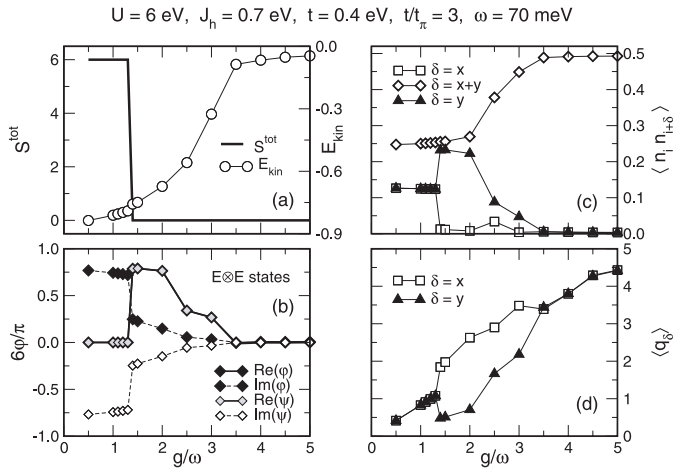

Fig. 11. Doping $x = 0.5$: (a) Total spin and kinetic energy *vs.* g; (b) complex orbital states on diagonal bonds; (c) density-density correlations; (d) lattice distortion $\langle q_\delta \rangle$ in x and y direction.

proportional to t^2/J_h, gains importance. Consequently FM order is unstable at much lower g, if compared to the case $x = 0.25$. The FM to AFM transition is not connected to charge localisation and causes only a tiny jump of the kinetic energy (see Fig. 11a).

The calculated orbital correlations are interesting as well. On a diagonal bond the most probable $E \otimes E$-eigenstate of the reduced orbital density matrix is symmetric for all considered values of g, $|s(\varphi, \psi)\rangle$. Note however, that the associated angles are *complex* conjugated $\varphi = \psi^* \in \mathbb{C}$ within both the FM and parts of the AFM phase (see Fig. 11b). This result reminds of some recent mean-field studies [42–45], which obtain different patterns of complex orbital ordering, in particular within the ferromagnetic conducting phase. Of course, our exact data for a finite cluster does not relate to any complex long range order. It shows, however, that complex linear combinations of the states $|\theta\rangle$ and $|\varepsilon\rangle$ could be the appropriate choice for an approximate description of the complicated orbital correlations observed within the metallic phase of the manganites. As soon as a large electron phonon coupling g causes charge localisation real orbital states are again favourable (*cf.* Fig. 11b).

In Figure 12 we summarise the behaviour of the lattice, the spins and the orbitals. With growing g the cluster expands isotropically until a finite x-y-distortion develops at the FM to AFM transition (see also Figure 11d). Further increase of g causes the carriers to localise and the distortion to disappear. The spin background undergoes a change from FM order to different types of AFM order. Of course, within the four site system we are not able to detect more complicated spin arrangements like the CE-type order observed experimentally [30]. However, the sensitivity of the system to small changes in the model parameters is clearly visible. Note that the depicted orbitals represent the amplitude of the underlying complex states $|\varphi\rangle$.

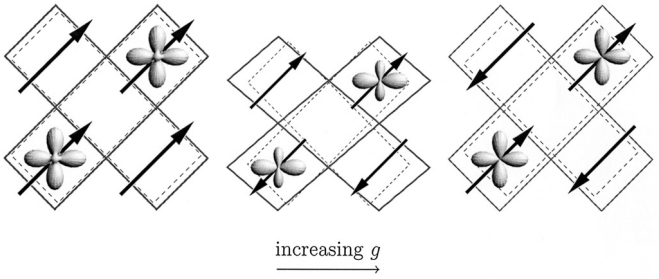

Fig. 12. Evolution of lattice, spin and orbital correlations with increasing electron-phonon coupling g at doping $x = 0.5$.

4 Conclusion

In the present work we have derived a microscopic model for doped CMR manganites which includes the dynamics of charge, spin, orbital, and lattice degrees of freedom on a quantum mechanical level. Using exact diagonalisation techniques we have studied how the electron-lattice interaction affects short range spin and orbital correlations. An observation, which is important for the understanding of the undoped compounds, is the suppression of the spin-orbital coupling with increasing electron-phonon interaction. For the weakly doped compounds we have demonstrated the direct relationship between the trapping of charge carriers and the breakdown of ferromagnetism. In addition, we have shown that changes in the spin correlations are reflected in dynamic lattice correlations. At intermediate doping we find that the system depends on a subtle balance of double-exchange, superexchange and electron-lattice interaction. The latter enhances the tendency for charge ordering which in turn affects spin and orbital order. Besides the calculation proves that complex orbital states can be a suitable approximation for the description of orbital correlations. Although the calculated data is not quantitatively comparable to real, three dimensional materials, the exact diagonalisation of even a small system provides detailed insight into correlations and driving interactions behind the rich phase diagram of the manganites. In addition, the exact results may support the development of approximate theories.

We thank L.F. Feiner, F. Göhmann, D. Ihle, G. Khaliullin, and J. Loos for valuable discussions. The grant of computational resources by HLR Stuttgart and NIC Jülich, as well as financial support by the Deutsche Forschungsgemeinschaft and the Czech Academy of Sciences is acknowledged.

References

1. R.M. Kusters, J. Singleton, D.A. Keen, R. McGreevy, W. Hayes, Physica B **155**, 362 (1989)
2. R. von Helmolt, J. Wecker, B. Holzapfel, L. Schultz, K. Samwer, Phys. Rev. Lett. **71**, 2331 (1993)
3. S. Jin, T.H. Tiefel, M. McCormack, R.A. Fastnach, R. Ramesh, L.H. Chen, Science **264**, 413 (1994)

4. J.M.D. Coey, M. Viret, S. von Molnár, Adv. Phys. **48**, 167 (1999)
5. Y. Tokura, Y. Tomioka, J. Magn. Magn. Mater. **200**, 1 (1999)
6. E. Dagotto, T. Hotta, A. Moreo, Phys. Rep. **344**, 1 (2001)
7. C. Zener, Phys. Rev. **82**, 403 (1951)
8. P.W. Anderson, H. Hasegawa, Phys. Rev. **100**, 675 (1955)
9. K. Kubo, N. Ohata, J. Phys. Soc. Jpn **33**, 21 (1972)
10. A.J. Millis. Nature **392**, 147 (1998)
11. S. Ishihara, J. Inoue, S. Maekawa, Physica C **263**, 130 (1996)
12. R. Shiina, T. Nishitani, H. Shiba, J. Phys. Soc. Jpn **66**, 3159 (1997)
13. R. Maezono, S. Ishihara, N. Nagaosa, Phys. Rev. B **57**, R13993 (1998)
14. L.F. Feiner, A.M. Oleś, Phys. Rev. B **59**, 3295 (1999)
15. J.S. Griffith, *The Theory of Transition-Metal Ions* (Cambridge University Press, Cambridge, 1971)
16. P.W. Anderson, Phys. Rev. **115**, 2 (1959)
17. K.I. Kugel, D.I. Khomskii, JETP Lett. **15**, 446 (1972)
18. A. Weiße, J. Loos, H. Fehske, Phys. Rev. B **64**, 054406 (2001)
19. Y. Tanabe, S. Sugano, J. Phys. Soc. Jpn **9**, 766 (1954)
20. J. Zaanen, G.A. Sawatzky, J. Solid State Chem. **88**, 8 (1990)
21. A.E. Bocquet, T. Mizokawa, T. Saitoh, H. Namatame, A. Fujimori, Phys. Rev. B **46**, 3771 (1992)
22. T. Mizokawa, A. Fujimori, Phys. Rev. B **51**, 12880 (1995)
23. M. Quijada, J. Černe, J.R. Simpson, H.D. Drew, K.H. Ahn, A.J. Millis, R. Shreekala, R. Ramesh, M. Rajeswari, T. Venkatesan, Phys. Rev. B **58**, 16093 (1998)
24. *The Dynamical Jahn-Teller Effect in Localized Systems*, Vol. 7 in Modern Problems in Condensed Matter Sciences, edited by Yu.E. Perlin, M. Wagner (North-Holland, Amsterdam, 1984)
25. T. Holstein, Ann. Phys. (N.Y.) **8**, 325 (1959)
26. M.N. Iliev, M.V. Abrashev, H.-G. Lee, V.N. Popov, Y.Y. Sun, C. Thomsen, R.L. Meng, C.W. Chu, J. Phys. Chem. Solids **59**, 1982 (1998)
27. W. Reichardt, M. Braden, Physica B **263-264**, 416 (1999)
28. A. Weiße, H. Fehske, G. Wellein, A.R. Bishop, Phys. Rev. B **62**, R747 (2000)
29. J.K. Cullum, R.A. Willoughby, *Lanczos Algorithms for Large Symmetric Eigenvalue Computations*, Vols. I & II (Birkhäuser, Boston, 1985)
30. E.O. Wollan, W.C. Koehler, Phys. Rev. **100**, 545 (1955)
31. F. Moussa, M. Hennion, J. Rodriguez-Carvajal, H. Moudden, L. Pinsard, A. Revcolevschi, Phys. Rev. B **54**, 15149 (1996)
32. D.D. Sarma, N. Shanthi, S.R. Barman, N. Hamada, H. Sawada, K. Terakura, Phys. Rev. Lett. **75**, 1126 (1995)
33. W.E. Pickett, D.J. Singh, Phys. Rev. B **53**, 1146 (1996)
34. S. Satpathy, Z.S. Popović, F.R. Vukajlović, Phys. Rev. Lett. **76**, 960 (1996)
35. I. Solovyev, N. Hamada, K. Terakura, Phys. Rev. Lett. **76**, 4825 (1996)
36. K.I. Kugel, D.I. Khomskii, Sov. Phys. JETP **37**, 725 (1973)
37. G. Khaliullin, V. Oudovenko, Phys. Rev. B **56**, R14243 (1997)
38. L.F. Feiner, A.M. Oleś, J. Zaanen, J. Phys. Cond. Matt. **10**, L555 (1998)
39. Y. Murakami, J.P. Hill, D. Gibbs, M. Blume, I. Koyama, T. Tanaka, H. Kawata, T. Arima, Y. Tokura, K. Hirota, Y. Endoh, Phys. Rev. Lett. **81**, 582 (1998)
40. C.H. Booth, F. Bridges, G.H. Kwei, J.M. Lawrence, A.L. Cornelius, J.J. Neumeier, Phys. Rev. Lett. **80**, 853 (1998)
41. R. Kilian, G. Khaliullin, Phys. Rev. B **60**, 13458 (1999)
42. D. Khomskii (2000), URL `http://arXiv.org/abs/cond-mat/0004034`
43. A. Takahashi, H. Shiba, J. Phys. Soc. Jpn **69**, 3328 (2000)
44. R. Maezono, N. Nagaosa, Phys. Rev. B **62**, 11576 (2000)
45. J. van den Brink, D. Khomskii, Phys. Rev. B **63**, 140416 (2001)